

## **A NOVEL TERAHERTZ SENSING DEVICE COMPRISING OF A PARABOLIC REFLECTIVE SURFACE AND A BI-CONICAL STRUCTURE**

**M. Cai and E. P. Li**

Advanced Electronics and Electromagnetics Group  
Institute of High Performance Computing  
Singapore

**Abstract**—A sensing device comprising of a parabolic reflective surface and a bi-conical metal structure is proposed to focus terahertz energy on sample material in the sensing zone to create a strong interaction between terahertz signals and the sample under test. The signal enhancement by the sensing device is confirmed by modeling and simulation results. The proposed sensor is applied to investigate the polarization dependency of a split ring resonator (SRR), and spectral signatures of the SRR under different incident wave polarizations are obtained.

### **1. INTRODUCTION**

Terahertz (THz) sensing technology has received considerable attention in recent years for its potential applications in the detection of biological materials, skin cancer and spectral signature for molecular vibrations in RNA, DNA strands or proteins [1–7]. In those applications, the material properties such as the dielectric constants, loss tangent and conductivities may be extracted. Some materials, especially biological materials may cause absorption of THz energy for certain frequency due to their unique molecular structures and environment conditions. The spectral responses of the biomaterials obtained can be used as the signature of such materials to identify same material in real test in the same conditions.

THz Time-Domain (THz-TD) technology has been used for THz sensing and the spectral responses of the sample under test can be obtained over a wide frequency range since a pulse signal with rich

---

Corresponding author: M. Cai (caimao@ihpc.a-star.edu.sg).

frequency components is applied to the sample and the scattered signal from the sample material is then captured to give the spectral response of the sample under test for identification and clarification.

Interaction between THz energy and sample material is the key for THz sensing. Typically, the sample material is located in the path way between a THz source and a detector. In this case, the sample material interacts with a THz wave from the source and the forward scattered wave is received by a THz detector [1, 4, 5]. Attenuated total reflection (ATR) is also introduced for THz sensing while the THz beam is redirected by a prism toward the sample material [3]. The THz wave is totally reflected and received by the detector. In this case, the sample material interacts with the evanescent wave along the surface of the prism created by the total reflection of the THz beam.

The output power of THz signal generated by photoconductive antenna is very low due to the low conversion efficiency (in the order of  $10^{-4}$ ) from the exciting laser power to THz radiation. The noise figure of THz detector by photoconductive antenna is high, so that a high signal to noise ratio (SNR) is required to extract the THz signal from the signal received. Parabolic mirrors have been widely used in THz systems to focus the weak THz power to the sample to increase the SNR [1–6]. On the other hand, a bi-conical structure has been widely used as a broadband radiation device with very high field concentration at gaps between the conical structure [12, 13]. This motivates us to study on THz sensing device to achieve high energy concentration in the sensing zone to increase the interaction between the THz wave and the sample under test, by using a combination of a parabolic mirror and a bi-conical structure.

In this paper, we proposed a THz sensing device consisting of a parabolic metal surface and a bi-conical metal structure. The bi-conical structure is located with the focus point of the parabolic surface and the axis of the bi-conical structure is parallel to the surface of the parabolic surface. The dimension of the sensing device and its radiation property are described in Section 2, and the simulation approach and results to show the strongest  $E$ -field in the sensing area are presented in Section 3. Split ring resonators (SRR) have been investigated extensively as a potential metamaterial structure with a negative refractive index [8–11]. An SRR structure with strong resonance at the THz frequency range is used as a sample material to show the effectiveness of this proposed THz sensor in Section 4. The formula of signal processing to extract the spectral signature of the SRR response to incident THz wave is presented in Appendix A.

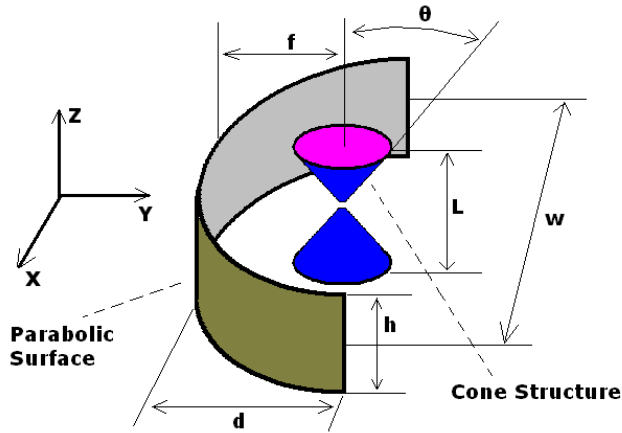


**Figure 1.** Configuration of the proposed THz sensing device.

## 2. PROPOSED THZ SENSING DEVICE

### 2.1. Configuration of THz Sensing Device

The configuration of the proposed THz sensing device is shown in Fig. 1. It consists of two components: a parabolic metal surface and a bi-conical structure. The cone structure is placed at the focus point, with its axis parallel to the parabolic surface.

The parabolic surface is to focus the incident THz wave from a THz source to the focus point of the parabolic surface. The  $E$ -field at the gap of the cone structure, which is also the focus point of the parabolic surface, is expected to be further enhanced by the cone structure. By placing sample material at the gap of the cone structure, strong interaction between THz wave and sample material is expected to occur.

The cone structure is designed as an antenna in the frequency range from 1 to 6 THz. The strong interaction between THz wave and the sample material at the gap is then radiated effectively by the cone structure, and reflected by the parabolic surface to the direction of a THz wave detector.

### 2.2. Radiation Efficiency of the THz Sensing Device

The radiation property of the THz sensing device is investigated by using XFDTD, a well known software tool for electromagnetic modeling and simulation. The bi-conical structure has a length of

$L = 100 \mu\text{m}$  and an angle of  $\theta = 45^\circ$ . The parabolic surface has a focus point with a distance of  $f = 100 \mu\text{m}$ , a depth of  $d = 225 \mu\text{m}$ , a height of  $h = 200 \mu\text{m}$  and a width of  $w = 600 \mu\text{m}$ . A mesh size of  $4 \mu\text{m}$  is used during the simulation. In the area around the gap of the cone structure, the mesh size is reduced to  $0.667 \mu\text{m}$  ( $1/6$ ) of normal mesh size by using the adaptive mesh scheme provided by XFDTD.

The gain at the  $y$  direction ( $\varphi = 90^\circ$ ,  $\theta = 90^\circ$ ) and the VSWR of the THz sensing device are shown in Fig. 2(a) when a Gaussian pulse is applied to the gap of the cone structure. It is observed that the antenna has a gain higher than 14 dBi and a VSWR lower than 3.0 over the frequency range of 2 to 6 THz. The radiation patterns at the  $XY$  plane ( $\theta = 90^\circ$ ) and the  $YZ$  plane ( $\varphi = 90^\circ$ ) are shown in Fig. 2(b). The maximum gain of 17 dBi is well matched with the results at Fig. 2(a). The THz sensing device is therefore confirmed to act as an effective antenna, which works very well to focus the THz wave from the THz source to the sample at the gap of the cone structure, and to radiate the signals generated by the strong interaction between the THz wave and the sample located at the gap back to the THz detector. It is also noted that the radiation pattern is sharp in the  $XY$  plane (with a 3 dB beam of  $5^\circ$ ) and quite broad in the  $YZ$  plane (with a 3 dB beam width of  $20^\circ$ ). The sharp beam in the  $XY$  plane are highly contributed by the parabolic surface.

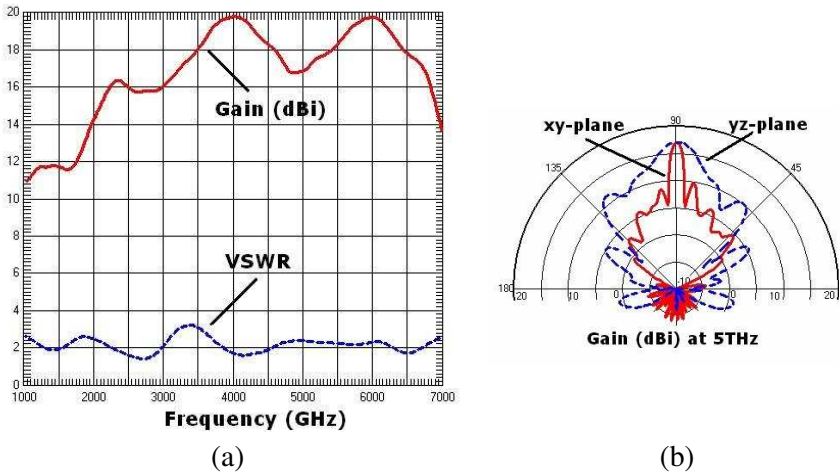


**Figure 2.** Radiation properties of the THz sensing device. (a) Gain and VSWR. (b) Radiation pattern.

### 3. SIGNAL ENHANCEMENT OF THE THZ SENSING DEVICE

#### 3.1. The System Configuration for the Investigation of Signal Enhancement

A virtual testing environment as shown in Fig. 3 is used to investigate the signal enhancement of the THz sensing device.

The proposed THz sensing device is used as an antenna for THz source and detector. In actual application, the photoconductive antennas for THz source and detector can be placed at the gaps of the THz sensing device. In the virtual testing environment, ideal THz source and detector are used.

The THz source and detector are placed with a distance of  $H = 200 \mu\text{m}$  in  $Z$  direction, and the THz sensing device is placed in a distance of  $R = 1000 \mu\text{m}$  from the source and detector in  $Y$  direction. The THz wave from the source is directed to the THz sensing device. The scattered field generated by the interaction of the incident THz wave and the sample at the sensing zone is then radiated back to the detector. The radiation properties of the THz sensing device as shown in Section 2 ensure that the THz wave from this source is well directed to the THz sensing device, and the scattered field from the THz sensing device is also well targeted to the THz detector. The direct coupling between the source and detector is then removed by a time-gating window.

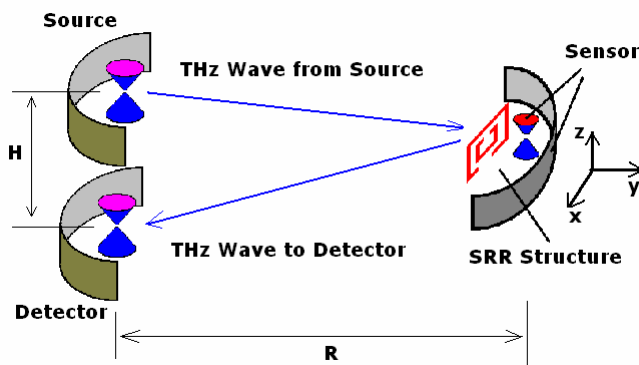


**Figure 3.** System configuration of a virtual testing environment.

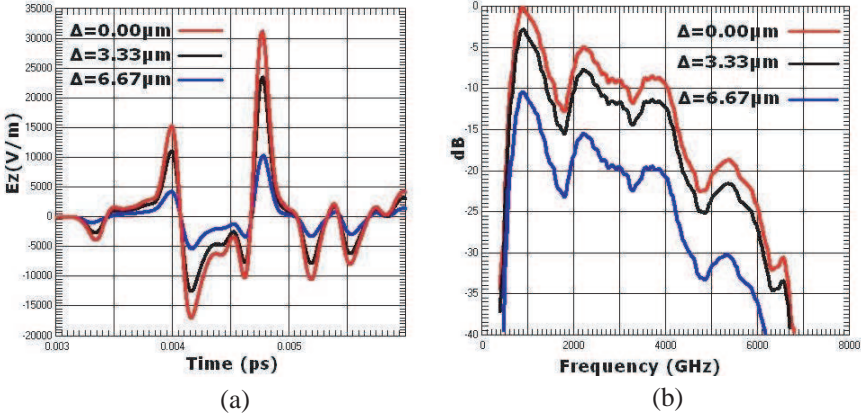


**Figure 4.** Near field signal strength in sensing zone. (a) Near field time domain signal strength in sensing zone. (b) Near field frequency domain signal strength in sensing zone.

### 3.2. Near Field Signal Enhancement at the Sensing Zone

The near field signal in the sensing zone is investigated by applying a Gaussian pulse at the gap of the cone structure of the THz source. The near field time domain signals of the  $E_z$  component in the sensing zone and their spectral signals in frequency domain with a distance  $\Delta = 0, 3.33$  and  $6.67 \mu\text{m}$  from the focus point, while there is no sample presence, are shown in Figs. 4(a) and (b), respectively. It is observed that the near field strength in both time domain and frequency domain is strongest in the centre, which is also the focus point of the parabolic surface. The gap of the bi-conical structure is  $4 \mu\text{m}$ , which may be adjusted according to the size and type of the sample under test.

The signal enhancement by the THz sensing device is confirmed by comparing the signal strength with the following cases:

- 1) Near field strength for the same location when the parabolic surface is removed (Cone Only);
- 2) Near field strength when the bi-conical structure is removed (Parabolic Surface Only);
- 3) Near field strength when both parabolic surface and bi-conical structure are removed (Free space).

In each case, the near field strength for the same location is integrated over the same period and expressed in dB scale.

The comparisons of the near field signal strength of the THz sensing device in the sensing zone are shown in Fig. 5. It is observed

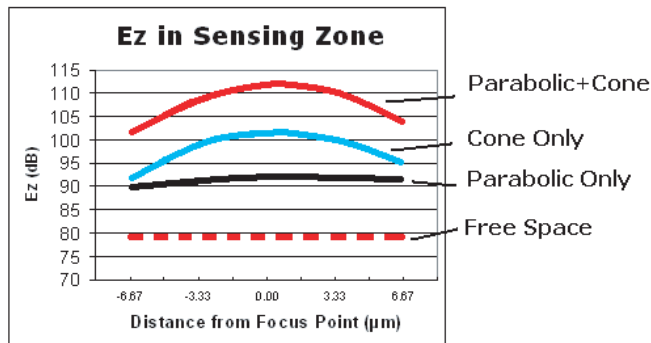


**Figure 5.** Near field strength comparisons in sensing zone.

that the parabolic surface and the bi-conical structure increase the near field strength for 10 dB and 20 dB with respect to the near field strength in free space, respectively. The joint effect of the parabolic surface and the bi-conical structure then achieves an enhancement of 30 dB in the strength of the near field.

It is also observed that the near field enhancement occurs only in the sensing zone, i.e., the gap and its surrounding. This shows this THz sensing device can be used to pinpoint to a very small area. And the size of the sensing zone can be adjusted by the size of the bi-conical structure.

#### 4. APPLICATIONS OF THE SENSING DEVICE FOR THE SPECTRAL SIGNATURE EXTRACTION OF SPLIT RING RESONATOR

##### 4.1. Split Ring Resonator (SRR)

The effectiveness of the THz sensing device is investigated by placing a unit cell of SRR structure in the  $X$ - $Z$  plane at the sensing zone with  $30\ \mu\text{m}$  distance from the bi-conical structure of the sensing device. The dimension of the SRR structure and its orientation with respect to the polarization of the incident THz wave are shown in Fig. 6. The polarization dependency of the SRR structure with respect to the polarization ( $E$ -field direction) of the incident THz wave is investigated by placing the gaps of the SRR structure in  $Z$  and  $X$  direction, while the polarization of the incident THz wave is in  $Z$  direction. The SRR structure in with gaps in  $Z$  and  $X$  directions is referred as  $Z$ -Sample and  $X$ -Sample, respectively.

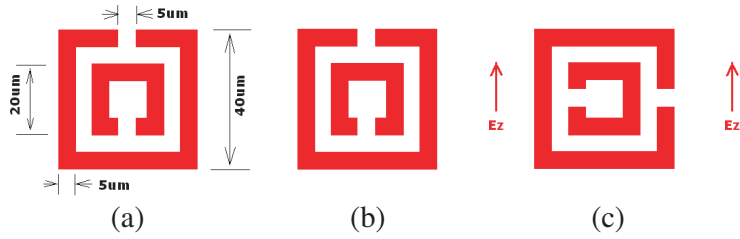


**Figure 6.** Dimensions of SRR structure and its orientations. (a) Dimensions of SRR structure. (b) The gaps of SRR structure in line with the polarization of incident THz wave ( $Z$ -Sample). (c) The gaps of SRR structure perpendicular to the polarization of incident THz wave ( $X$ -Sample).

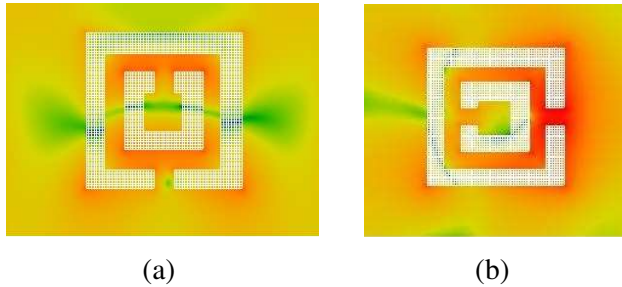


**Figure 7.**  $E$ -field spatial distribution of SRR. (a)  $E$ -field spatial distribution of  $Z$ -Sample. (b)  $E$ -field spatial distribution of  $X$ -Sample.

#### 4.2. $E$ -field Spatial Distribution of SRR

Figure 7 shows the  $E$ -field spatial distribution at the plane of SRR when an incident THz wave with  $E$ -field in the  $Z$  direction is used. It shows the  $E$ -field is highly concentrated at the gap between the rings of the SRR. And the highest  $E$ -field concentration or enhancement is at the gap of the split ring for  $X$ -sample, while the gaps of the split ring are perpendicular to the  $E$ -field direction of the incident THz wave.

Figure 8 shows that  $E$ -Field strength in both time domain and frequency for  $E$ -field at the gap of the outer ring of SRR structure. It is found that  $E$ -field at the gap of  $X$ -sample has a higher amplitude and the signal strength is more concentrate at the lower frequency end around 1000 GHz (1 THz), as compared with the  $E$ -field at the gap of  $Z$ -sample.

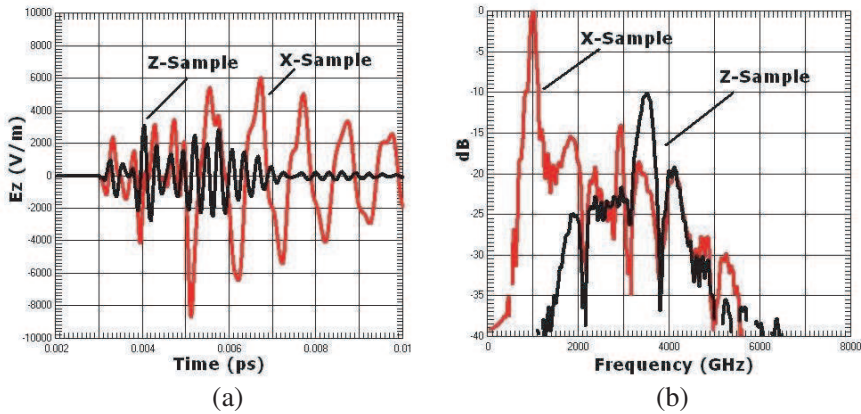


**Figure 8.**  $E$ -field signal strength at the outer gap of SRR. (a)  $E$ -field time domain signal at the outer gap of SRR. (b)  $E$ -field frequency domain signal at the outer gap of SRR.

### 4.3. Spectral Signatures of SRR

The spectral signatures for  $Z$ -Sample and  $X$ -Sample are obtained through procedures as follows.

- 1) Applying a Gaussian pulse at the source device when there is no sample in the sensing zone, the signal received at the detecting antenna is recorded as the calibration signal.
- 2) Applying the same Gaussian pulse as the calibration process at the source device when the SRR sample is placed in the sensing zone, the signal received at the detecting antenna is recorded as the total signal.
- 3) Deducting the calibration signal from the total signal at the detecting antenna, the signal contributed by the sample particle is obtained.
- 4) Applying the time-window to filter the unwanted signals appearing before or after the effective duration between the THz wave and the SRR sample, and conducting a Fourier transform to the time-gated signal, the spectral signature of the SRR sample in this measurement system is obtained.

The spectral signatures for  $Z$ -Sample and  $X$ -Sample of SRR structure are shown in Fig. 9. It is observed that the signature for  $Z$ -Sample has a single peak at 2 THz and the signature for  $X$ -Sample has two large peaks at about 0.8 and 3.5 THz, respectively. The signature

obtained at the detecting antenna is not a direction transformation of the near field signal at the outer gap of the SRR structure. It is also found the positions for peaks and nulls of the signatures for both  $Z$ -Sample and  $X$ -Sample match to each other quite well, but the height and depths of the peaks and nulls are different, due to the orientation of the SRR sample with respect to the polarization of the incident THz wave. This suggests that a serial of modes in the SRR structure are excited and those modes have different signals strength due to the polarization of the incident THz wave. The result shows that the SRR structure investigated has a high polarization dependency, and the spectral signature obtained can be used as identification for the orientation of the SRR structure. The formula to extract the spectral signature of the sample under test is shown in Appendix A.

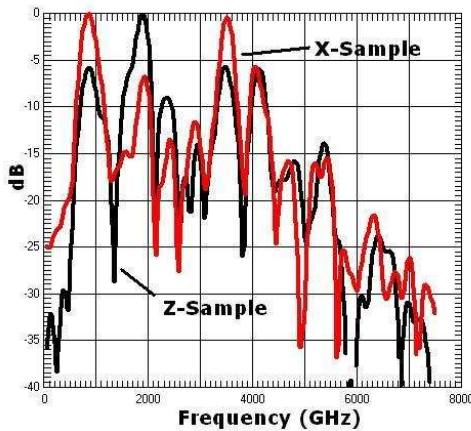


**Figure 9.** Spectral signature of SRR.

## 5. CONCLUSIONS

A novel type of THz sensing device is proposed and investigated using an FDTD approach. The modeling and simulation show that signal strength in the sensing zone is increased for more than 30 dB, and a strong interaction between the THz wave and the sample under test is therefore achieved as expected. The effectiveness of the proposed THz sensing device is demonstrated and proven by applied the THz sensing device to investigate the spectral signature of a split ring structure under different polarization of incident THz wave. The spectral signature shows that the SRR structure investigated has a strong dependency on the polarization of the incident THz wave.

Further investigation will be conducted on the optimization of the structure of the sensing device and the integration with actual THz time-domain sensing system.

## APPENDIX A. POST PROCESSING TO EXTRACT THE SPECTRAL SIGNATURE OF SAMPLE

At the sensing zone, the near field signal is disturbed if some samples are placed. The  $E$ -field of the total signal  $E_{Total}^{(1)}(t)$  can be expressed as

$$E_{Total}^{(1)}(t) = E_{REF}^{(1)}(t) + E_{sample}^{(1)}(t) + n^{(1)}(t) \quad (A1)$$

Here  $E_{REF}^{(1)}(t)$  is the  $E$ -field of the near field without the presence of sample material,  $E_{sample}^{(1)}(t)$  is the  $E$ -field generated by the interaction between the incident THz wave and the sample material, and  $n^{(1)}(t)$  is the noise from the system and environment.

At the detecting antenna, the  $E$ -field of the total signal  $E_{Total}^{(2)}(t)$  can be expressed as

$$E_{Total}^{(2)}(t) = E_{REF}^{(2)}(t) + E_{sample}^{(2)}(t) + n^{(2)}(t) \quad (A2)$$

Here the field components at the detecting antenna in Equation (2) are related to the field components at the sensing zone through the impulse response  $h(t)$  as follows.

$$E_{REF}^{(2)}(t) = \int_0^t E_{REF}^{(1)}(\tau)h(t-\tau)d\tau \quad (A3)$$

$$E_{Sample}^{(2)}(t) = \int_0^t E_{sample}^{(1)}(\tau)h(t-\tau)d\tau \quad (A4)$$

However, the noise signals  $n^{(1)}(t)$  and  $n^{(2)}(t)$  at sensing zone and the detecting antenna are somehow independent with each other, and are related to the testing or simulation environment.

In order to extract signal generated by the interaction of the THz and the sample materials, a calibration process is conducted by calculating the  $E$ -field strength  $E_{cali}^{(2)}(t)$  at the detecting antenna without the presence of sample material at the sensing zone.

$$E_{cali}^{(2)}(t) = E_{REF}^{(2)}(t) + n^{(2)}(t) \quad (A5)$$

By removal of the calibration signal from the total signal at the detecting antenna, we have

$$E_{sample}^{(2)}(t) = E_{Total}^{(2)}(t) - E_{cali}^{(2)}(t) \quad (A6)$$

The spectral signature for the sample material is then giving by

$$\begin{aligned} E_{sample}^{(2)}(j\omega) &= E_{Total}^{(2)}(j\omega) - E_{cali}^{(2)}(j\omega) \\ &= \int_{T1}^{T2} (E_{Total}^{(2)}(t) - E_{cali}^{(2)}(t)) \exp(j\omega t) dt \end{aligned} \quad (A7)$$

Here  $(T1, T2)$  is the time window applied to filter the unwanted signal appearing before of after the signal from samples in the sensing zone.

## ACKNOWLEDGMENT

This research is conducted as part of the THz Research Project (Project No. 0821410039) under Agency for Science, Technology and Research (A\*STAR), Singapore.

## REFERENCES

1. Fischer, B. M., M. Hoffmann, H. Helm, R. Wilk, F. Rotz, K. O. Thomas, M. Koch, and P. U. Jepsen, "Terahertz time-domain spectroscopy and imaging of artificial RNA," *Optics Express*, Vol. 13, No. 14, 5205–5215, July 11, 2005.
2. Zhong, H., R. S. Albert, and X. C. Zhang, "Identification and classification of chemicals using terahertz reflective spectroscopy focal plane imaging system," *Optics Express*, Vol. 14, No. 20, 9130–9141, October 2, 2006.
3. Hirori, H., K. Yamashita, M. Nagai, and K. Tanaka, "Attenuated total reflection spectroscopy in time-domain using terahertz coherent pulses," *Japanese Journal of Applied Physics*, Vol. 43, No. 10A, L1287–L1289, 2004.
4. Huang, F., B. Schulkin, H. Altan, J. F. Federici, D. Gary, R. Barat, D. Zimdars, M. Chen, and D. B. Tanner, "Terahertz study of 1,3,5-trinitro-triazine by time-domain and fourier transform infrared spectroscopy," *Applied Physics Letters*, Vol. 85, No. 23, 5535–5537, December 6, 2004.
5. Usami, M., M. Yamashita, K. Fukushima, C. Otani, and K. Kawase, "Terahertz wideband spectroscopic imaging based on two-dimensional electro-optic sampling technique," *Applied Physics Letters*, Vol. 86, No. 14, 141109.1–141109.3, 2005.
6. Kitagawa, J., T. Ohkubo, M. Onuma, and Y. Kadoya, "THz spectroscopic characterization of biomolecule/water systems by

- compact sensor chips,” *Applied Physics Letters*, Vol. 89, No. 4, 041114.1–041114.3, July 26, 2006.
7. Hor, Y. L., J. F. Federici, and R. L. Wample, “Nondestructive evaluation of cork enclosures using terahertz/millimeter wave spectroscopy and imaging,” *Applied Optics*, Vol. 47, No. 1, 72–78, January 1, 2008.
  8. Rockstuhl, G., T. Zentgraf, H. Guo, N. Liu, C. Etrich, I. Loa, K. Syassen, J. Kuhl, F. Lederer, and H. Giessen, “Resonances of split-ring resonator metamaterials in the near infrared,” *Applied Physics B*, Vol. 84, 219–227, 2006.
  9. Han, J., A. Lakhtakia, and C. W. Qiu, “Terahertz metamaterials with semiconductor split-ring resonators for magnetostatic tunability,” *Optics Express*, Vol. 16, No. 19, 14390–14396, September 2008.
  10. O’Hara, J. F., R. Singh, I. Brener, E. Smirnova, J. Han, A. J. Taylor, and W. Zhang, “Thin-film sensing with planar terahertz metamaterials: Sensitivity and limitations,” *Optics Express*, Vol. 16, No. 3, 1786–1795, February 2008.
  11. Bitzer, A., H. Merbold, A. Thoman, T. Deurer, H. Helm, and M. Walther, “Terahertz near-field imaging of electric and magnetic resonances of a planar metamaterial,” *Optics Express*, Vol. 17, No. 5, 3826–3834, March 2009.
  12. Leithner, A. and C. P. Wells, “Radiation by disk and conical structures,” *IRE Trans. Ant. Propag.*, 637–640, October 1956.
  13. King, R., “The conical antenna as a sensor or probe,” *IEEE Trans. EMC*, Vol. 25, No. 1, 8–13, February 1983.